

## AE MONITORING FROM CVD-DIAMOND FILM SUBJECTED TO MICRO-INDENTATION AND PULSE LASER SPALLATION

**R.Ikeda**

*Asahi Diamond Industrial Co., Ltd, Chiba, Japan.,*

**H. Cho and M. Takemoto,**

*Aoyama Gakuin University, Kanagawa, Japan.,*

**K. Ono**

*UCLA, Los Angeles, USA*

### ABSTRACT

We monitored AEs during micro-indentation and pulse laser spallation test of CVD diamond film deposited on sintered SiC, and classified the fracture type by Lamb wave AE analysis.

In the indentation test with a Rockwell sphere indenter, we observed Hertz ring cracks and simultaneously detected AEs from Mode-I fracture. Crack types were classified from polarity distribution of the first arrival So-mode Lamb waves. Fracture strength of the diamond film was estimated as 7.1 GPa by FEM analysis, using the critical indentation force, indentation depth and Hertz crack diameter,

In the laser spallation test, strong pulse expansion-wave was produced by the pulse laser ablation of the confined silicone grease on the opposite surface of the diamond film and utilized to cause Mode-I delamination of diamond film. Critical tensile stress to cause the spallation was calculated as 222 MPa. We attempted to detect the spallation initiation by monitoring the in-plane motion of So-mode Lamb wave AE using broad-band pinducer mounted on the edge planes. Waveform change due to the Mode-I spallation was detected.

**KEYWORDS:** Diamond film, Indentation test, Ring crack, Fracture strength, Laser spallation, Interfacial strength

### INTRODUCTION

CVD-diamond-coated tools are widely used for machining graphite, ceramics and Al-Si alloys.

Wear performance of diamond film as a cutting tool has been demonstrated to be excellent. However decohesion (fracture) of the film during machining has been remained as problem. This problem is more serious than the antifriction problem of the film. In order to study the fracture mechanism, fracture strength of the film and film/substrate interface must be correctly evaluated.

Indentation fracture test using spherical indenter gives us a lot of useful information about micro-fracture characteristics. When this test is applied to hard material, Hertz ring crack is caused by the surface tensile stress given by the Hertz theory [1]. Fracture strength of ceramic coating have been evaluated using the threshold load to cause the first ring crack and FEM analysis [2,3]. Here, accurate determination of crack initiation load is critical. We monitored progression of micro-cracks during loading using AE system. We classified fracture types by analyzing the polarity distribution of the first arrival So-mode Lamb wave. This AE system is different from the conventional AE system utilized for indentation [4,5] and scratch test [6,7].

We developed a pulse laser spallation method to measure the absolute adhesion strength of hard coatings. It utilizes strong shock waves produced by pulse laser breakdown of confined grease or liquid. For the measurement of adhesive strength, scratching and indentation methods have been adopted so far [8],[9],[10], but could not measure the absolute adhesion strength. The strength estimated by these conventional methods changes depending on the testing conditions, such as the surface roughness, shape and stiffness of the indenter. Furthermore these methods can hardly be applied to diamond film. Contrary to this, laser spallation technique [11] can estimate the Mode-I adhesion strength when both the out-of-plane displacement of expansion wave and critical laser energy to cause micro spallation are correctly measured.

We first conducted Rockwell indentation test to CVD-diamond film to estimate the fracture strength of the film, then estimated interfacial adhesion strength of the film utilizing the pulse laser spallation technique. AE was successfully utilized for damage detection and fracture mode classification.

**EXPERIMENTAL**

**INDENTATION TEST**

We prepared polycrystalline diamond film with grain size of 10 to 20 μm deposited on sintered SiC substrate by hot-filament CVD method of 3 % methane and 97 % hydrogen gas mixture. The films were polished using diamond wheel to obtain a clear indentation and spallation of the diamond film.

Experimental setup for the indentation test is shown in Fig. 1. We used a Rockwell indenter with spherical tip (radius: 0.2 mm and angle: 120 degree) . Maximum indentation loads : $F_{max}$  were changed at 98, 196, 294, 392 and 490 N. Loading

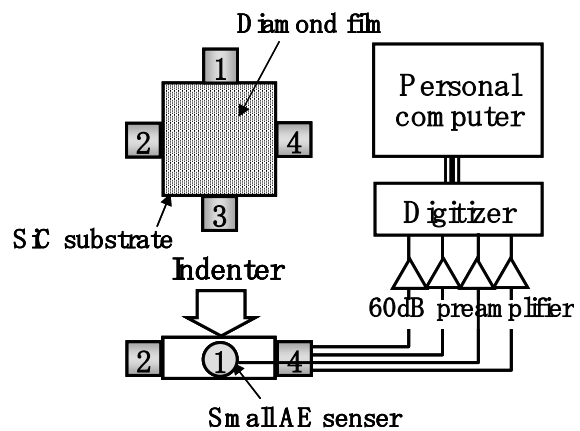


Fig. 1 Experimental setup for the indentation test and AE monitoring.

rate and holding time are controlled to be 0.49 N/s and 10 s, respectively. Four small PZT-type AE sensors (PAC, Type PICO, center frequency :500 kHz) were mounted on the four edge surfaces of the substrate. Sensor outputs were amplified by 60 dB using a pre-amplifier (NF9913, NF Circuit Co.), digitized by a fast A/D converter (Compu Scope, CS12100 Gage Applied Sciences Inc.) and fed to a personal computer. Sampling interval and sampling points were set as 50 ns and 2048, respectively. Diamond film of 35  $\mu\text{m}$  thickness on 5 mm thick SiC of 20 mm square was submitted to the test. Thus the AE system monitors the Lamb (or plate) wave AEs. We classified fracture modes or crack types by analyzing the polarity distribution or radiation pattern of So-mode Lamb wave. Two types of crack, the Mode-I fracture with a crack opening vector parallel to the surface corresponding to the ring crack, and the Mode-II fracture or lateral crack at the film/substrate interface, were classified. Detail of polarity distribution analysis can be found elsewhere [12]. It is noted that all polarities of So-mode are positive for the Mode-I crack, but two opposite polarities for the Mode-II crack.

### LASER SPALLATION TEST

Experimental setup for the laser spallation is shown in Fig. 2. A high-energy Q-switched pulse Nd:YAG laser (New Wave Research, Tempest300, maximum energy: 300 mJ, pulse duration time: 3-5 ns, wavelength: 1064 nm) was irradiated on the opposite surface of the diamond film. Silicone grease containing fine MoS<sub>2</sub> particles was painted on the surface as an energy-absorbing layer. Thickness of the layer was controlled precisely using a

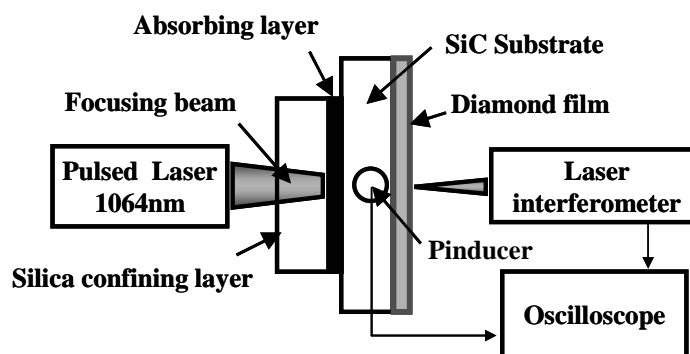


Fig. 2 Experimental setup for laser spallation and AE monitoring.

thickness gage of 20  $\mu\text{m}$  and confined rigidly by a 6-mm-thick silica plate with anti-reflection coating. Impact wave was excited by the laser breakdown of the grease. The beam diameter was controlled to be 1 mm by changing the defocusing distance. Laser energy was changed from 0.7 to 63 mJ. Diamond film with 78  $\mu\text{m}$  thickness deposited on 35 mm square and 5.0 mm thick SiC substrate was tested. A heterodyne-type laser interferometer (He-Ne laser, 532 nm) was used to measure the out-of-plane displacement of the stress wave at the epicenter of the source. In order to detect the spallation initiation, small AE sensor (Valpey Fisher, pinducer ,6.0 MHz) was glued on the end surface of the specimen. Sensor to source distance was kept as 14.5 mm. Leak laser was used as trigger signal for the laser interferometer and AE system. Signals were digitized and stored in a high-resolution digital oscilloscope at sampling interval of 0.4 ns with sampling points of 8192. Output of the AE sensor was directly fed to the digital oscilloscope.

**RESULTS AND DISCUSSION**

**SPHERICAL INDENTATION TEST**

We observed frequent ring crack generation during the indentation test. Number of ring cracks increased with maximum indentation load  $F_{max}$  and expanded into outward area of the first ring crack. Figure 3 (a) shows the indentations produced by the test of  $F_{max}$ : 98 N, and (b) the indentation curve (indentation force  $F$  vs. indentation depth  $h$ ) with AE timings. We detected frequent AE signals from the Mode-II fracture (open triangles). These AEs were, however, considered to be the contact noise. Only one Mode-I AE, from the ring crack was detected as indicated by solid triangle at 39.1 N. The number of the Mode-I AEs increased with  $F_{max}$ . Here we focused our attentions on the load to cause the first ring crack in order to evaluate the tensile strength of the diamond film. Table 1 shows the load at which the first Mode-I AE was detected. The load was almost the same, except that (127.4 N) for  $F_{max}$ =196 N. AE signals from the Mode-I ring crack at the load of 39.1 N for  $F_{max}$ =98N are shown in Fig. 4. Polarities of first So mode was all positive, and indicate the initiation of Mode-I Hertz crack.

Next we calculated the film stress at the load of 39.1 N by FEM. Figure 5 (a) shows the axial

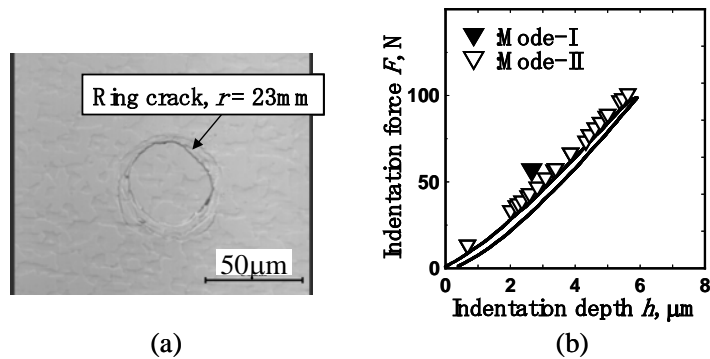


Fig. 3 Laser microscopic image of indentation (a) and indentation curve with AE timings (b), for the test of  $F_{max}$ : 98N.

Table 1 Load at the first Mode-I AE event.

$F_{max}$ [N]	98	196	294	392	490
Load at First Mode-I AE [N]	39.1	127.4	38.1	40.7	41.4

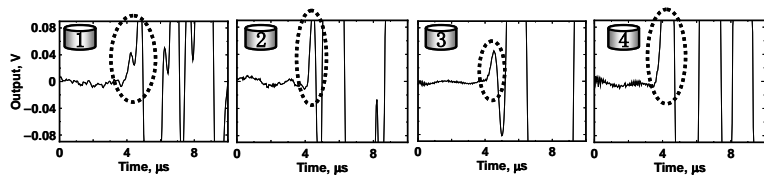


Fig. 4 AE waves from the Mode-I Hertz crack during the indentation test of  $F_{max}$ : 98N.

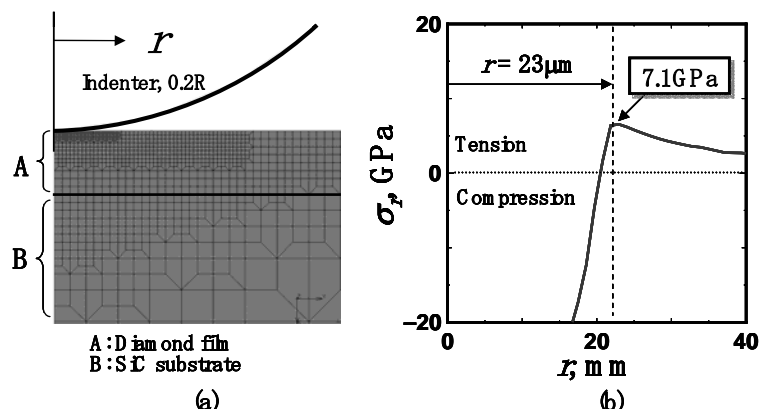


Fig. 5 Analysis model for FEM (a) and calculated stress distribution (b).

symmetric model for the FEM. We calculated the film stress for the indentation depth of 2.7  $\mu\text{m}$  at 39.1 N. Elastic properties of the CVD-diamond measured by laser ultrasonic technique [13] were used. Figure 5 (b) shows the distribution of radial stress. The maximum tensile stress is computed as 7.1 GPa to the contact radius of 23  $\mu\text{m}$ . This radius is consistent with the measured radius in Fig. 3. Thus the tensile fracture strength of the CVD-diamond film was estimated to be 7.1 GPa.

**LASER SPALLATION TEST**

Preliminary test showed that the diamond film suffers spallation at laser energy of around 46 mJ. Figure 6 shows microscopic images of spallated area. Spallation occurred above laser energy of 46.1 mJ. We observed very small delamination of 0.3 mm diameter at 46.1 mJ, though not clear in the photo. Delaminated circle expanded with laser energy. In order to estimate the adhesion strength correctly, we must determine the delamination initiation. Owing to the transparency of the polished diamond film, we can detect the spallation by eye inspection when a finite size delamination occurs, however, much accurate detection technique is needed for non-transparent and rough surface films.

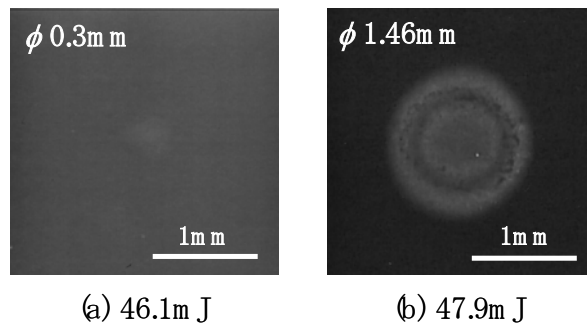


Fig. 6 Optical microscopic images of spallation.

We are now using two method. One is waveform analysis from the interferometer. Figure 7 compares the outputs of laser interferometer for the case of spallation (b) and no-spallation (a). There observed very clear waveform difference at first portion of the P-waves. Wave oscillation of 28-33 ns cycle in (a) is due to the multi-reflection of the P-wave (1400 m/s) in the confined grease layer. This oscillation disappears when spallation occurs.

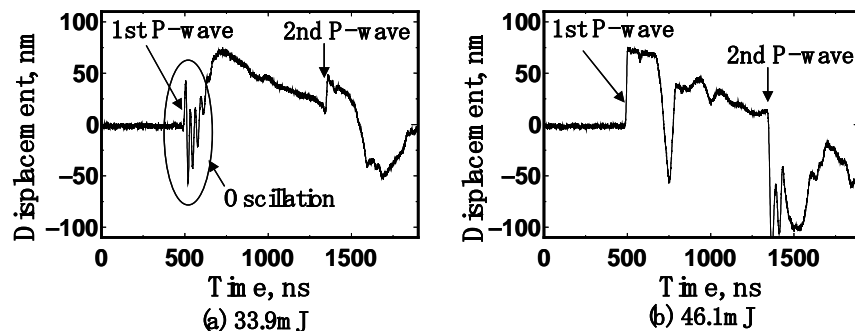


Fig. 7 Bulk waves detected by laser interferometer at just epicenter of oil breakdown, (a) without spallation and (b) with spallation.

This is because the reflected P-wave can not be transmitted to the delaminated film. In this case, the film spallation was induced by the first arrive P-wave. We next estimated the critical interfacial stress to cause spallation. We detected out-of-plane displacement of the stress wave at just epicenter on the substrate. Figure 8 shows the waveforms as a function of laser power from 4.8 to 47.9 mJ. At low energies from 4.8 to 15 mJ, the compressive wave or down shooting wave is the major component. The expansion component appears above 35.5 mJ and increases with laser energy. Tensile stress of the expansion component is given by Eq.

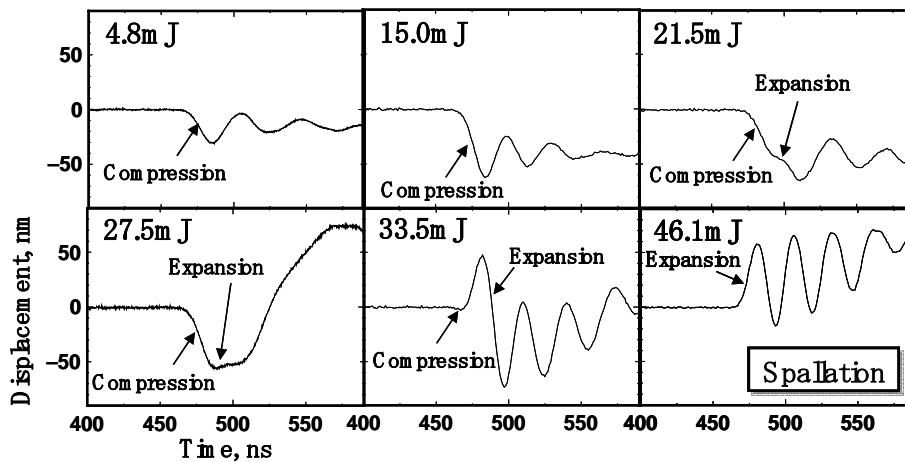


Fig. 8 Change of first arrival bulk wave from oil breakdown, detected for SiC substrate without the film.

(1) [14].

$$\sigma = -\rho V_l \frac{\partial u(t)}{\partial t} \tag{1}$$

where  $\rho$  is the density of the medium and  $V_l$  denotes the velocity of the longitudinal wave.  $\rho$  and  $V_l$  of sintered SiC are taken as  $3150 \text{ kg/m}^3$  and  $11803 \text{ m/s}$ , respectively. The partial differentiation of displacement with respect to time defines the particle velocity of the longitudinal wave. Figure 9 shows the stresses calculated for compression (●) and expansion (○) waves. Here compressive stress was designated by minus symbol. Tensile stress increased with increasing the laser energy. Data scattering appears to be due to the difficulty in determination of the particle velocities. The adhesive strength of the diamond film is estimated as 222 MPa.

In order to determine the spallation initiation accurately, we utilized AE monitoring. We previously detected the impact-induced cracks in the PMMA hit by flying objects [15]. For such case, weak AE by fracture is hidden by strong impact induced AE and could not be detected by the AE sensor mounted on the plate surface. We, however, could monitor the fracture-induced weak AE by monitoring the in-plane motion of the So-Lamb waves using the sensors mounted on the edge plane of the target [15]. We used this technique and detected Lamb-wave AE from the spallation using the pinducer mounted on the edge plane.

Figure 10 shows detected Lamb wave AE as a function of laser energy. Arrival time of the first So-mode coincides the calculated arrival time of So-mode AE from the breakdown of silicone at

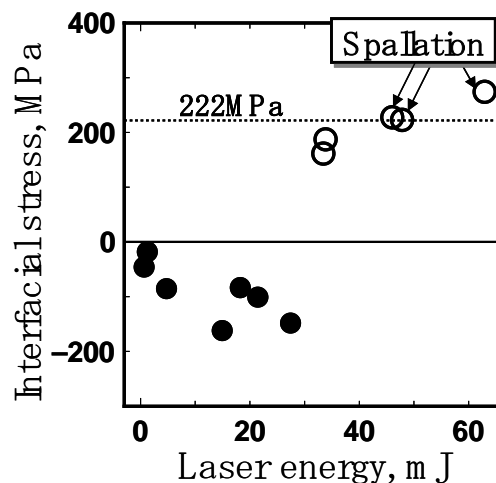


Fig. 9 Interfacial Stresses by pulse wave due to the oil-breakdown.

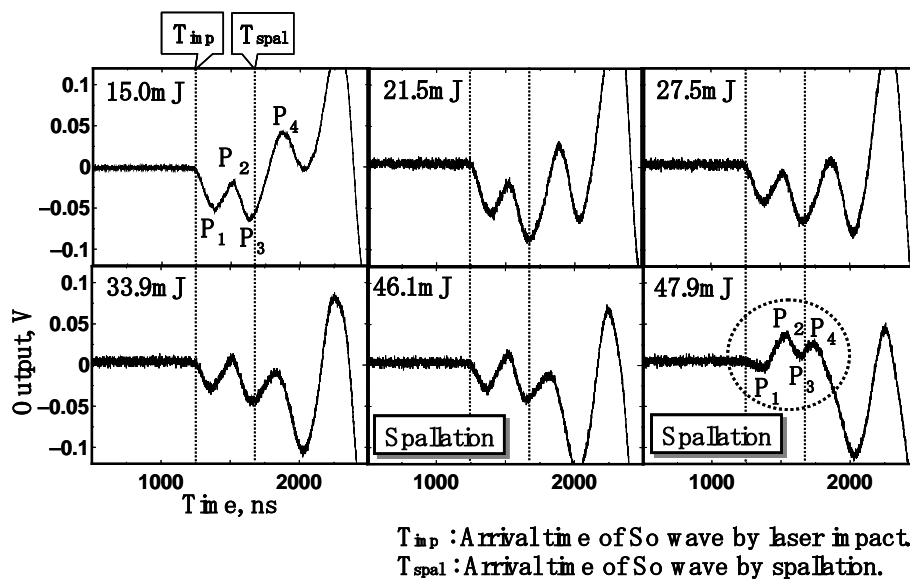


Fig. 10 First component of So-lamb waves detected by the pinducer mounted on edge place on SiC with the film.

the sheet velocity of 11,585 m/s. This timing is shown by a vertical line at  $T_{imp}$ . Another vertical line indicated by  $T_{spal}$  predicts the arrival time of the first So-mode AE from the spallation. Arrival time of first three peaks,  $P_1$ ,  $P_2$  and  $P_3$ , do not change for any laser energies, but their amplitude and polarity changes with laser energy. This means that the kinetics of oil breakdown does not change. A small spallation of 0.3 mm diameter occurred at the energy of 46.1 mJ. Waveform at 47.9mJ is so much different from other waves. Both the polarity and amplitude of  $P_3$  and  $P_4$  wave significantly changed at 47.9 mJ. Plus polarity of  $P_4$  wave indicates the Mode-I spallation. Cross-correlation factor of these waves is shown in Fig.

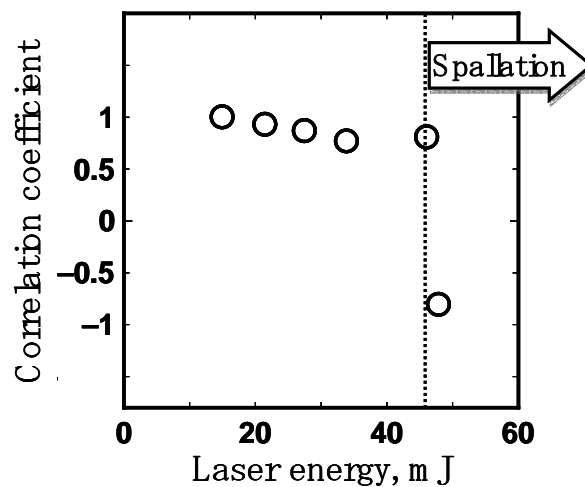


Fig. 11 Cross correlation coefficients of waveform at in Fig. 10.

11 as a function of laser energy. It shows a sharp change at 47.9 mJ which produce large spallation.

CONCLUSION

We utilized AE for detecting and classifying the film fractures during Rockwell micro-indentation and laser spallation test of CVD-diamond films deposited on the SiC plate. Results are

summarized below:

- 1) Mode-I Hertz ring crack during Rockwell indentation was detected by advanced AE system utilizing four AE sensors around the indenter. Critical indentation load, indentation depth and ring crack diameter to cause the first Hertz crack were determined and submitted to FEM analysis. Tensile strength of the diamond film was estimated to be 7.1 GPa.
- 2) Laser spallation technique makes it possible to determine the absolute interfacial strength of CVD-diamond film on SiC substrate by measuring the fast out-of-plane displacement of the expansion stress wave. Adhesion strength was estimated as 222 MPa.
- 3) In order to detect the spallation initiation, we monitored in-plane motion of the So-mode Lamb wave by broad band small sensor (pinducer) mounted on the distal planes. The sensor detected the AE from large spallation.

## ACKNOWLEDGEMENT

This research was conducted as part of the High-Technology Research Center Program and the Center of Excellence (COE) Program, funded by the Ministry of Education, Culture, Sports, Science and Technology of Japan.

## REFERENCES

- [1] H. E. Powell and F. W. Preston, *J. Amer. Ceram. Soc.*, **28**, 6, (1945) 145.
- [2] H. Kagawa, M. Ichikawa, T. Takamatsu and H. Kuwano, *Trans. J. Soc. Mech. Eng. A60*, 570 (1994), 396.
- [3] K. Hayashi and Y. Fang, *Trans. J. Soc. Mech. Eng. A60*, 617 (1998), 30.
- [4] M. Shiwa, E. R. Weppelmann, A. Bendeli, M. V. Swain, D. Munz and T. Kishi, *Sur. Coat. Technol.*, 68/69 (1994), 598.
- [5] Y. Tsukamoto, H. Kuroda, A. Sato and H. Yamaguchi, *Thin Solid Films*, 213 (1992), 220.
- [6] P. A. Steinmann and H. E. Hintermann, *J. Vac. Sci. Technol.*, A3(6) (1985), 2394.
- [7] C. Julia-Schmutz and H. E. Hintermann, *Sur. Coat. Technol.*, 48 (1991) 1.
- [8] P. J. Burnett and D. S. Rickerby: *Thin Solid Films* **157** (1998) 233.
- [9] C. Julia-Schmutz and H. E. Hintermann: *Sur & Coat. Tech.* **48** (1991) 1.
- [10] P. C. Jindal, D. T. Quinto and G. J. Wolfe: *Thin Solid Films* **154** (1987) 361.
- [11] R. Ikeda, S. Tasaka, H. Cho and M. Takemoto, *Jpn. J. Appl. Phys.*, to be published.
- [12] A. Yonezu, T. Ogawa and M. Takemoto, *Progress in Acoustic Emission XI* (2002) 86-93.
- [13] R. Ikeda, Y. Hayashi and M. Takemoto, *Progress in Acoustic Emission XI* (2002), 53.
- [14] V. Gupta, J. Yuan and D. Martinez, *Surf. Eng. Struc. Ceram.* **76** (1993) 305.
- [15] H. Tanabe, Y. Mizutani and M. Takemoto, *J. Jpn. Soc. Non destructive inspection*, **53**, 4 (2004), 230.